Supplementary materials

Spatial distribution of motor endplates and its adaptive change in skeletal muscle

Xiaofeng Yin[1#], Tingting Yu[2,3#], Bo Chen[1], Jianyi Xu[2,3], Wentao Chen[1], Yisong Qi[2,3], Peixun Zhang[1], Yusha Li[2,3], Yuhui Kou[1], Yilin Ma[2,3], Na Han[1], Peng Wan[2,3], Qingming Luo[2,3], Dan Zhu[2,3*], Baoguo Jiang[1*]

1. Department of Trauma and Orthopaedics, Peking University People's Hospital, Beijing 100044, China

2. Britton Chance Center for Biomedical Photonics, Wuhan National Laboratory for Optoelectronics, Huazhong University of Science and Technology, Wuhan 430074, China

3. MoE Key Laboratory for Biomedical Photonics, Collaborative Innovation Center for Biomedical Engineering, School of Engineering Sciences, Huazhong University of Science and Technology, Wuhan 430074, China

[#]These authors contributed equally to the manuscript.

* Corresponding authors: Prof. Baoguo Jiang, jiangbaoguo@vip.sina.com and Prof. Dan Zhu, dawnzh@mail.hust.edu.cn

Supplementary Figures
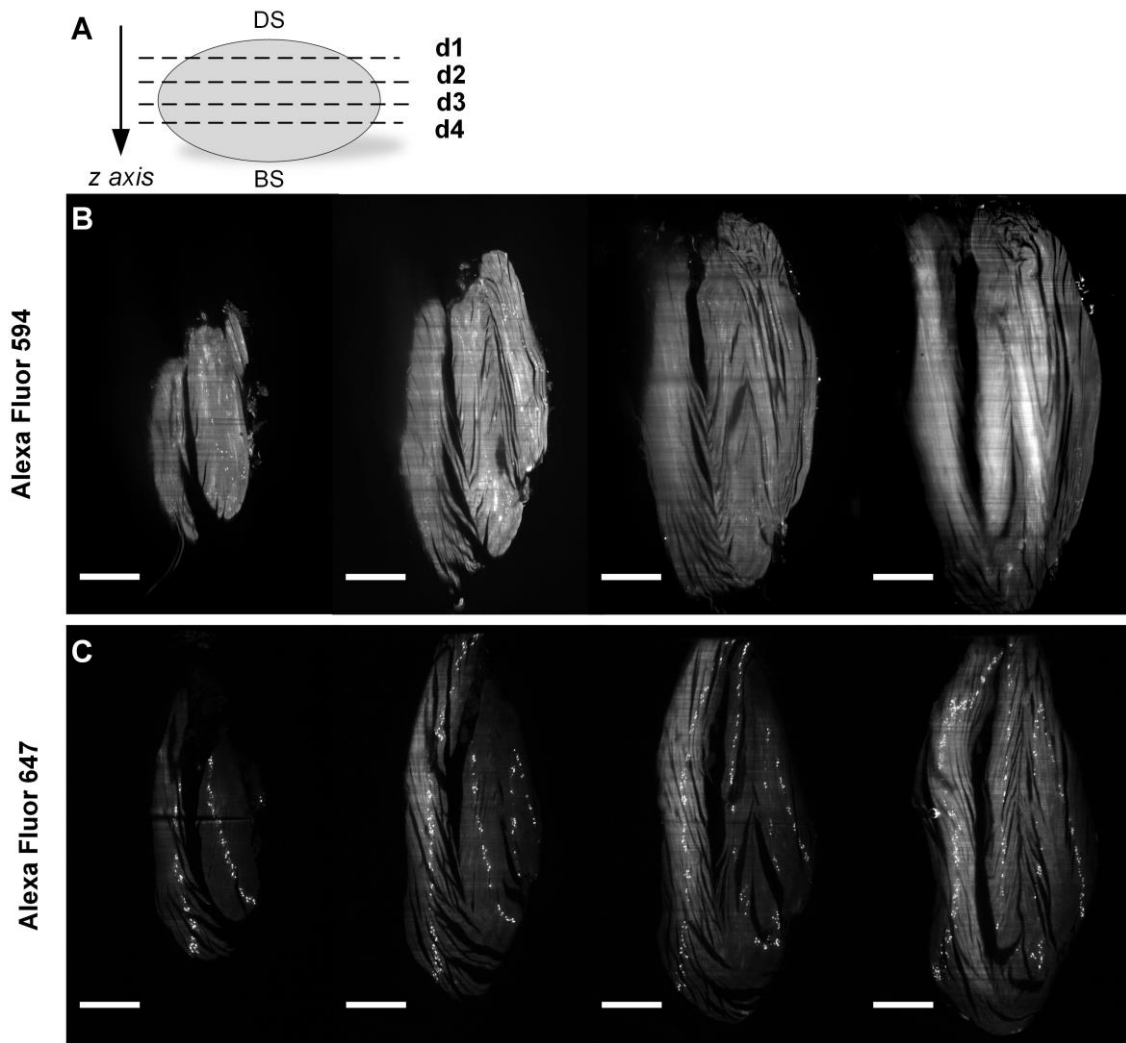
Figure S1. Autofluorescence using α-BTX conjugated with different fluorophores. (**A**) Schematic diagram of the locations for the images shown in **B** and **C**. (**B-C**) Z-section images of the gastrocnemius labeled with Alexa Fluor 594-conjugated α-BTX (**B**) and Alexa Fluor 647-conjugated α-BTX (**C**). The imaging planes shown here are similar. Note that the background autofluorescence in the muscle is minimized when using Alexa Fluor 647-conjugated α-BTX. BS: bone surface; DS: dorsal surface. d1-d4; different z depth. Scale bar, 1000 μm.
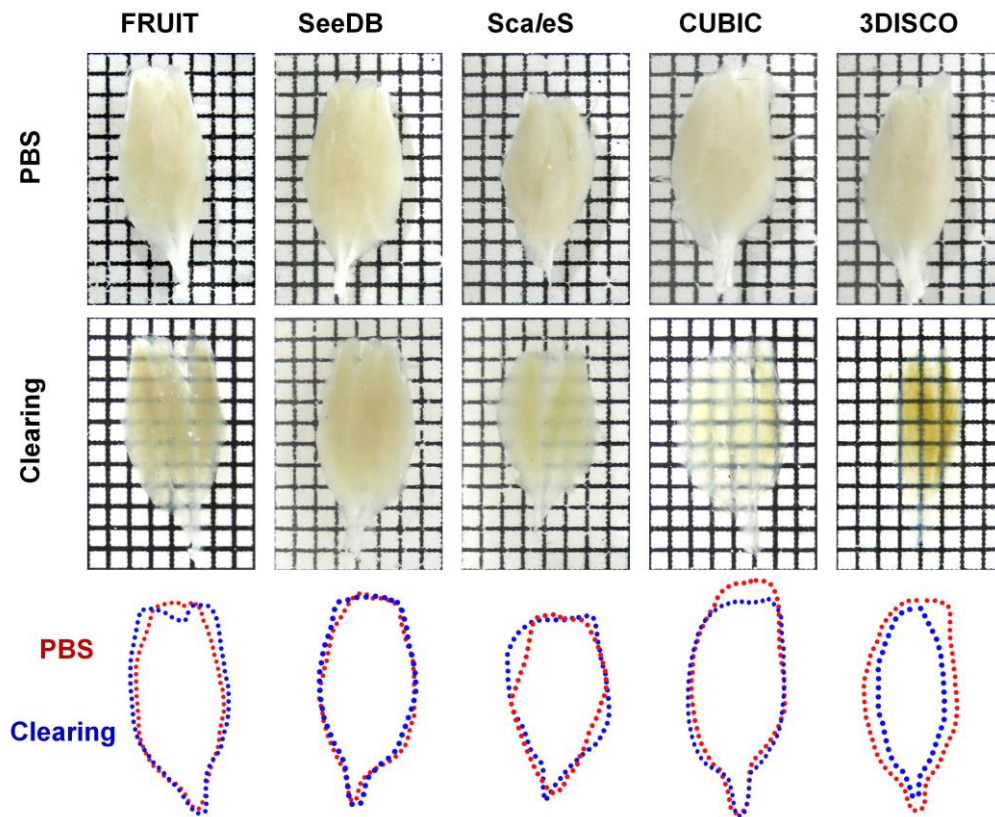
**Figure S2. Transparency of gastrocnemius cleared with different clearing protocols.** To identify the most efficient clearing protocol for skeletal muscles, we tested five clearing protocols, i.e., FRUIT, SeeDB, Sca*l*eS, CUBIC and 3DISCO. Among them, 3DISCO demonstrated the best transparency, and the induced shrinkage was helpful for imaging large-volume muscles. Grid size: 1.45 mm $\times$ 1.45 mm.
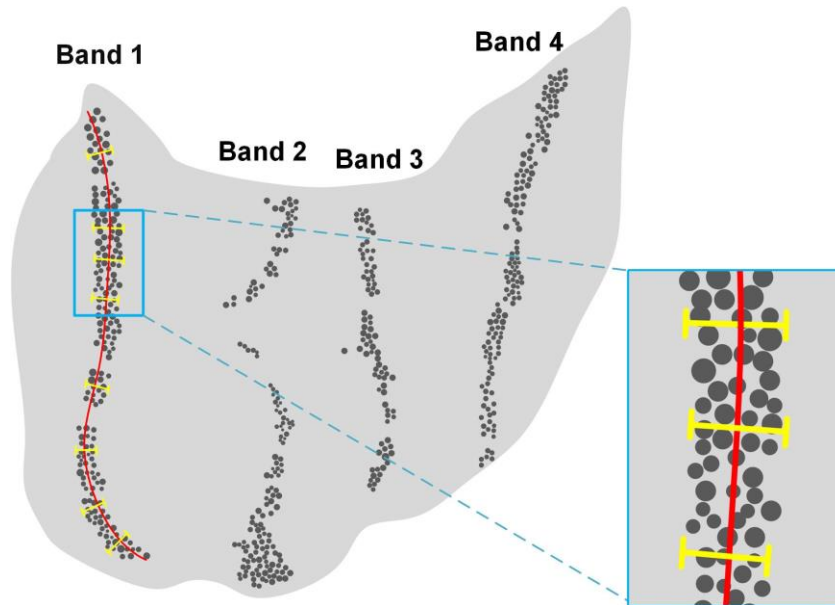
Figure S3. Schematic diagram for measurement of the width of one MEP band. To measure the width of the lamella clusters, we resampled the image stacks and obtained the cross-sectional images of gastrocnemius. Then, the maximum-intensity projections of Z-stacks (thickness = 200 μm) were made with ImageJ. For each band, five to ten positions were measured, and the maximum value of each band was used for averaging to calculate the band width of the MEPs.
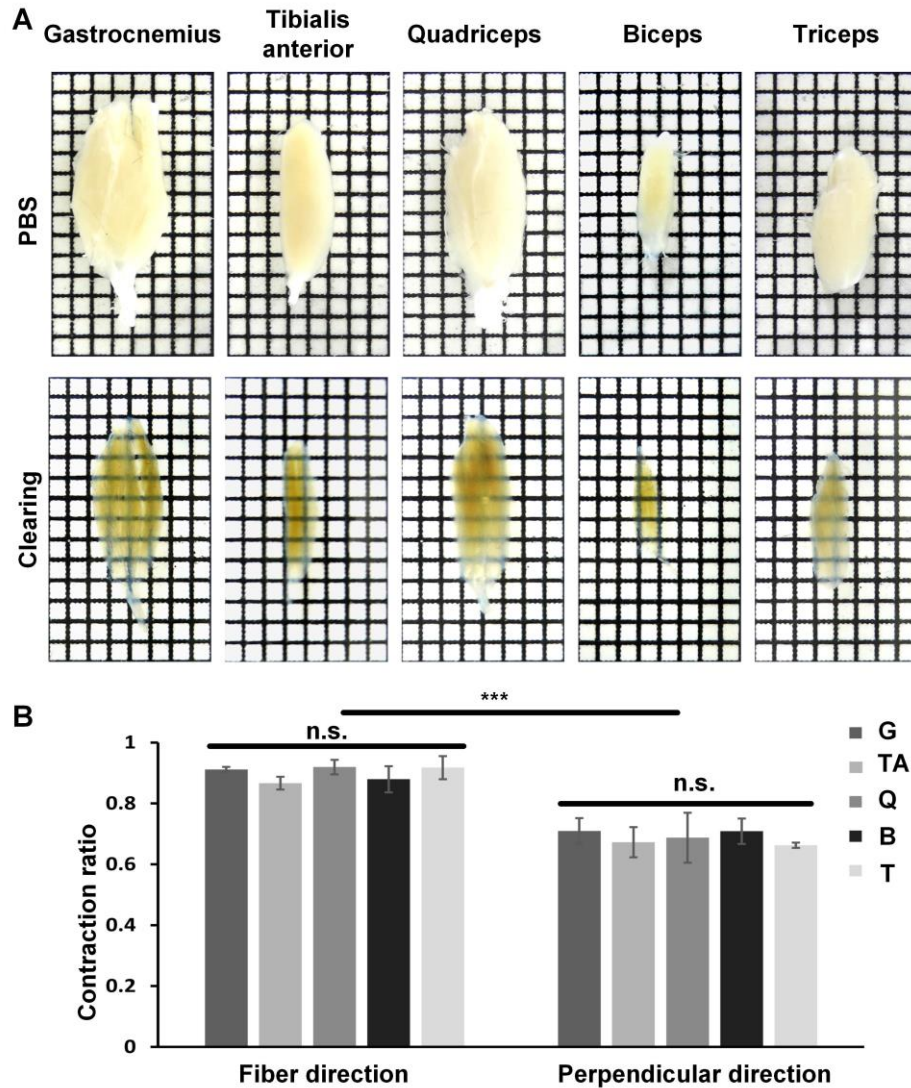
Figure S4. Different skeletal muscles before and after 3DISCO clearing. (**A**) Gross morphology of different muscles before and after clearing. Grid size, 1.45 mm×1.45 mm. (**B**) Quantifications of the contraction ratio in the fiber direction and the perpendicular direction. Data are presented as the mean ± s.d. One-way ANOVA was used for statistical analysis of the differences between different muscles. The paired t-test was used to compare the differences in the averages between the two directions. Note that there was no significant difference among the five muscles in either direction. The contraction in the muscle fiber direction and perpendicular direction were significantly different, which was due to the muscle fibers' arrangement. B, biceps; G, gastrocnemius; Q, quadriceps; T, triceps; TA, tibialis anterior.
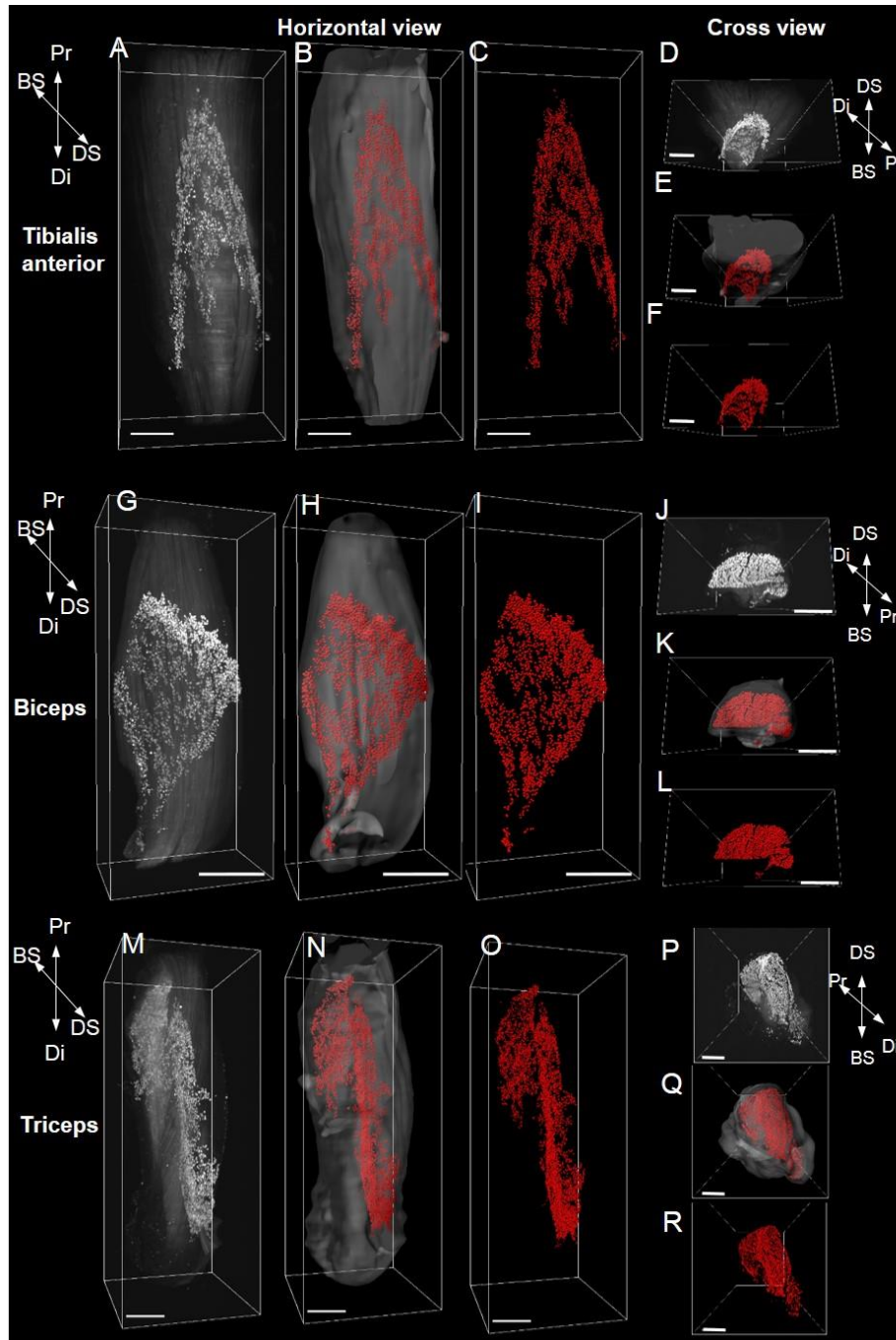
Figure S5. Three-dimensional distribution of MEPs in the tibialis anterior, biceps, and triceps.

Horizontal-sectional and cross-sectional views of raw image stacks (white), segmentation of muscle surfaces (light gray) and MEPs (red) for the tibialis anterior (**A**-**F**), biceps (**G**-**L**), and triceps (**M**-**R**). BS, bone surface; Di, distal end; DS, dorsal surface; Pr, proximal end. Scale bar, 1000 μm.
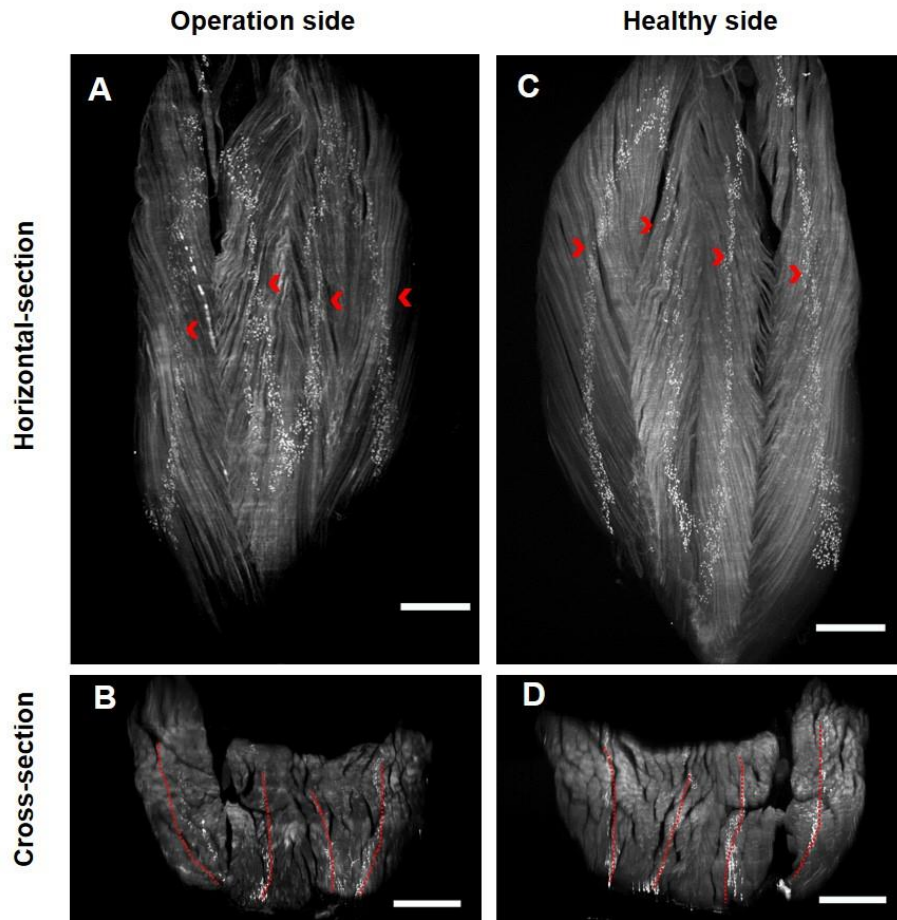
Figure S6. Distribution of MEPs in gastrocnemius after one-year recovery in tibial nerve repair model. Maximum-intensity projection of image stacks (thickness = 600 μm) and corresponding cross-sections (thickness = 200 μm) from the operation side (**A, B**) and healthy side (**C, D**). The lamella clusters of MEPs are indicated with red arrowheads in the horizontal sections and red dotted lines in the cross-sections. Scale bar, 1000 μm. After one-year recovery, the lamella clusters of MEPs in the gastrocnemius on the operation side were distributed in the same pattern as the healthy side.
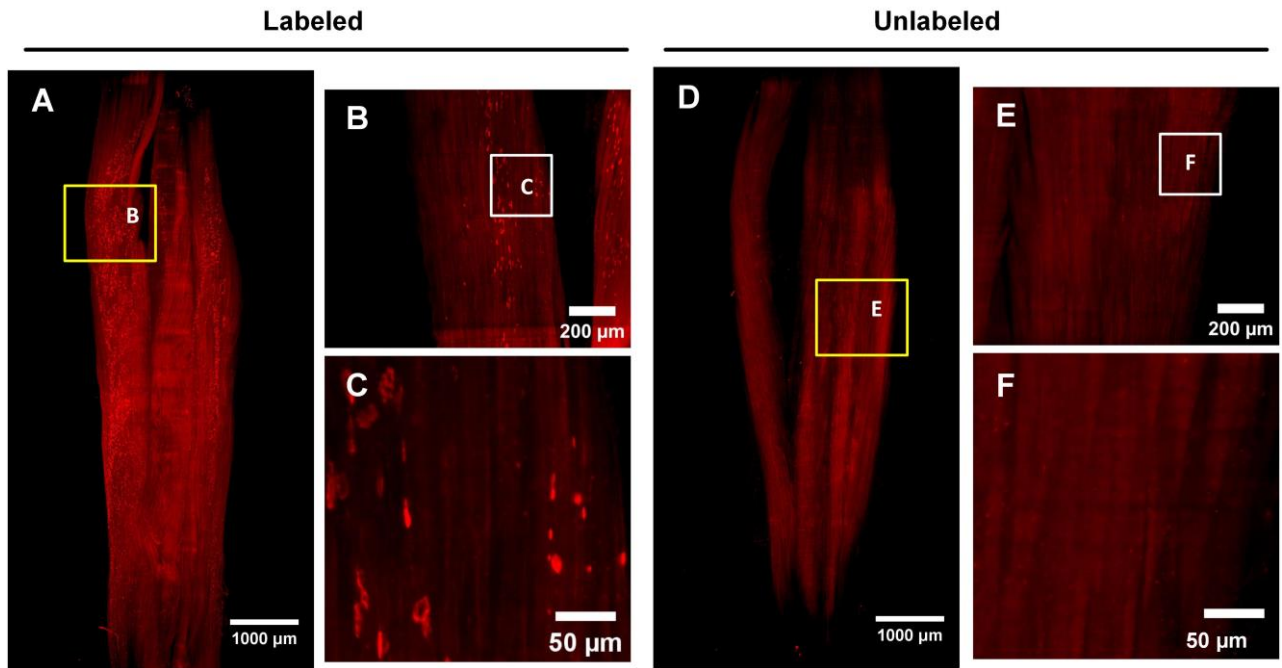
Figure S7. Validation of α-BTX labeling in denervated muscles. One month after the sciatic nerve transection, the mice were labeled with α-BTX (**A-C**) or unlabeled (**D-F**). Then, the gastrocnemius muscles were dissected, cleared and imaged with Ultramicroscopy. Maximum-intensity projection of light-sheet image stacks and the high-magnification views in the boxed regions are shown. The unlabeled muscle does not present any bright spots with strong signals, but these were present in labeled muscle.

Supplementary Videos

Supplementary Video Legends

Videos S1-5

Three-dimensional rendering and segmentation of MEPs in the gastrocnemius (Video S1), tibialis anterior (Video S2), quadriceps (Video S3), biceps (Video S4), and triceps (Video S5). The MEPs were labeled with Alexa Fluor 647-conjugated α-BTX. Muscles were imaged with the Ultramicroscopy, and animations were created with Imaris. The videos show different views of raw image stacks (white) and segmentations of muscle contour (light gray) and MEPs (red).

Videos S6-10

Visualization of MEPs and tracing of the nerve branches in the gastrocnemius (Video S6), tibialis anterior (Video S7), quadriceps (Video S8), biceps (Video S9), and triceps (Video S10). After imaging the nerve branches using the YFP signal (from *Thy1*-YFP-16 line mice) and MEPs through the *in vivo* injection of Alexa Fluor 647-conjugated α-BTX via the tail vein, we reconstructed the images with Imaris. The videos show different views of raw image stacks (white) and segmentations of MEPs (red) and nerve branches (green).

Video S11

Muscle contraction activities when electrically stimulating each nerve branch in the gastrocnemius. The muscle contraction activities in the areas of medial MEP lamella (MML) and lateral MEP lamella 1 (LML1) were observed when electrically stimulating the medial nerve branch (MNB) and lateral nerve branch 1 (LNB1), respectively. The muscle contraction activities of lateral MEP lamella 2 (LML2) and lateral MEP lamella 3 (LML3) were recorded by stimulating lateral nerve branch 2

(LNB2) and lateral nerve branch 3 (LNB3) together, and then only the muscle contraction of LML2 was induced after transecting LNB3.

Video S12

Three-dimensional reconstructions of MEPs in the denervated gastrocnemius over time. After labeling with Alexa Fluor 647-conjugated α-BTX, the gastrocnemius was cleared and imaged. The images were reconstructed using Imaris. The videos show different views of raw image stacks (left, white) and segmentations (right) of muscle contour (light gray) and MEPs (red).